National University of Science and Technology
POLITEHNICA București
Doctoral School of Industrial Engineering and Robotics

DOCTORAL THESIS ABSTRACT

Marcel ILIE

Computational studies of the aero-thermodynamics of supersonic propulsion systems

BUCHAREST 2023

Computational studies of the aero-thermodynamics of supersonic propulsion systems

Table of contents

Chapter 1 Background and literature review

1.1 Aircraft classifications

The aviation industry has a quite long history, and over the past century various aircrafts designs and technologies were developed and implemented. Therefore, a main classification of aircraft can be made based on the flying vehicles weight. It is important to note here that the aircrafts lighter than the air are classified as aerostats, while aircrafts heavier than air are classified as aerodynes. From the aerodynamic performance and utility point of views, the aerodynes received the most attention and interest from the aeronautical industry over the past century.

Figure 1.1 Schematic of a glider plane [149]

The aerodynes work by using the airflow which is pushed in one direction and thus, according to the Newton's third law of motion, thrust is generated. Fixed wings and rotorcrafts have been the most explored and developed aircraft carriers over the past century, and this was due to their applications and utility. It is important to mention here that the fixed wing generates the lift, needed for the fly, using the aerodynamic shape of the wing by creating a pressure differential between the lower and upper surfaces of the wing, while the aircraft moves through the air. On the

other hand, the rotorcraft generates lift by the rotating blades, and also by creating a pressure differential at the lower and upper surfaces of the blade. A further classification of fixed wing aircrafts is presented in Figure 1.2. Therefore, a very first classification of the fixed wing aircrafts can be made as powered and unpowered fixed wing aircrafts. The unpowered fixed wing aircrafts consists of gliders, paragliders, hang, sailplane, kite, etc. Figure 1.3 presents the schematic of a glider plane.

The classification of the powered aircrafts is more complex due to the fact that it consists of several categories. Therefore, a very first classification of the powered aircrafts can be made based on the number of wings and therefore, the aircrafts can be mono-plane, bi-plane or tri-plane. The powered flight has a long history which starts with the Wright brothers that designed, build and flew the first powered flight in 1903. It is worth to mention here that the first aircraft gas turbine engine was developed by Frank Whittle in 1930. This gas turbine engine development was followed relatively soon by the work of Hans-Joachim Pabst von Ohain who developed the turbojet engine in 1936. It is important to mention here that both Whittle and von Ohain are recognized as the first inventors of the air-breathing gas turbine engine. Air-breathing propulsion has been explored for more than a century for both subsonic and supersonic flights. It is worth to mention here that the subsonic air-breathing propulsion has been used in commercial aircraft carriers for more than a century.

Usually, the classification of the aircrafts can be made based on their wing geometry as: (i) fixed geometry, (ii) variable wing geometry (swept-back wings) and (iii) tailless aircrafts. It is worth to mention here that the swept-back or delta wings are used for high-speed (supersonic) aircrafts such as military aircrafts. Also, it is worth to mention here that the high-speed (supersonic) aircrafts use thin wings with low or no camber airfoil geometry such as NACA 0012-NACA0015 airfoil series.

Additional aircraft classification can be made based on the type of the wing as: (i) blended wing body (BWB) and (ii) hybrid wing body (HWB). A schematic of the flying wing aircraft is presented in Figure 1.4. This type of aircraft exhibits a high stability and aerodynamic performance and a relatively high maneuverability. Figure 1.5 shows the blended wing body (BWB) aircraft. As shown in Figure 1.5, the blended-wing body aircraft exhibits distinctive design and aerodynamic features when compared with the conventional aircrafts. Therefore, in the blended-wing aircraft, the fuselage and wing blend together and there is no distinct geometrical separation

between the aircraft fuselage and its wings. Moreover, the blended-wing aircraft design may or may not exhibit a tail.

Figure 1.2 Schematic of flying-wing aircraft [150]

Figure 1.3 Schematic of flying-wing aircraft [151]

The blended-wing body aircraft presents a couples of advantages such as increase lift and aerodynamic performance due to its extended lifting area, reduced drag. Also due to the fact that it can generate high lift, its size can be reduced compared with other wing aircraft configurations. Also, due its compact aerodynamic configuration, the blended wing body presents high aerodynamic stability.

1.2 Subsonic aircraft engines

The turbojet engine is schematically shown in Figure 1.12. The turbojet may use either axial or centrifugal compressors. It is worth to mention here that the first turbojet engine used centrifugal compressor for the compressor stage, while axial compressor design was used for the turbine stage. The compressors consist of stator-rotor stages and their number is defined by the power outcome required by the thrust conditions. As shown in Figure 1.12, the axial compressor and turbine stage consists of several blades rows. It is worth to mention here that some of the blades are stationary, while other are rotating. The stationary blades form the stator stage, while the rotating blades form the rotor stage. It is important to mention here that the turbojet engines are suitable for high subsonic flights. However, the turbojet engine can operate even at supersonic speeds and this is achieved by the addition of an afterburner. The afterburner enables additional of fuel injection which results into additional thrust. It is worth to mention that switching off the afterburner, the turbojet operates as a basic turbojet. Over time, it has been shown that the turbojet is not an efficient engine form the point of view of fuel consumption, while exhibiting high-level noise. Concorde was the last airplane that used the turbojet engine. However, it is worth to mention here that the Concorde was able to be fuel efficient only when flying at Mach number M=2.

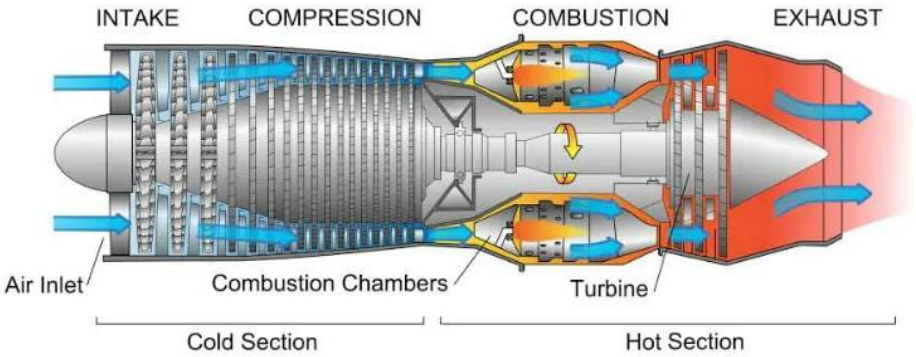

Figure 1.4 Schematic of turbojet engine [155]

1.3 Supersonic aircrafts

1.3.1 Introduction to ramjets

The first ramjet idea was proposed in 1913 by Rene Lorin. However, the lack of materials that can withstand the high temperatures developed from the combustion process, had postponed its physical development until 1949 when Rene Leduc designed the first ramjet. Therefore, Leduc was the first that designed the first ramjet powered aircraft, in 1949. However, the world's first flight powered by ramjet took place in 1939 and it was developed by Merkulov.

The ramjet is a jet engine that does not contains any rotating parts. Through its forward motion, it ingests the surrounding air and compress it through a passage duct. The compressed air is father delivered to the combustion chamber where the combustion process takes place. Since the ramjet does not have rotating parts that would enable the air ingestion, the ramjet cannot operate at zero air-speeds and therefore, it cannot provide the required thrust to move the aircraft. Therefore, the operation of the ramjet is conditioned by the flight speed and therefore, it requires to be carried by a different aircraft to reach a high Mach number speed to be able to ingest sufficient air required by the combustion process.

A schematic of the ramjet design and operation is shown in Figure 1.19. Generally, the ramjet comprises (i) inlet duct, (ii) combustion chamber and (iii) nozzle. The ramjet can operate on two types of fuel namely liquid and solid fuels. Also, it is worth to mention here that the ramjets can operate at both subsonic and supersonic speeds.

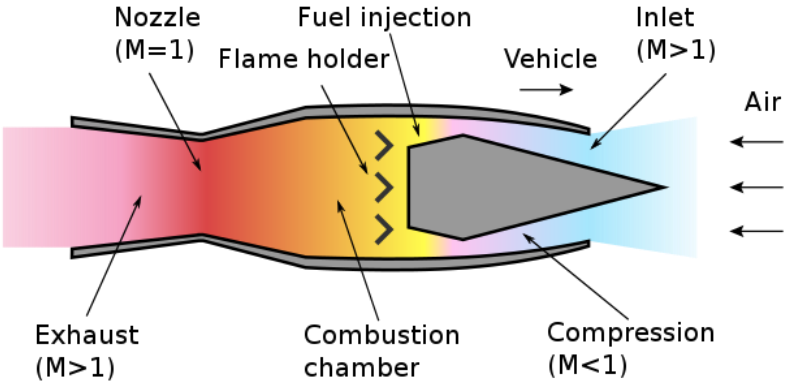

Figure 1.5 Schematic of ramjet engine [157]

In the schematic in Figure 1.19, the air enters the ramjet inlet from right to the left at supersonic speed (M>1). As the airflow enters the inlet region, the airflow is slowed down to subsonic regime by a series of oblique shocks generated by the interaction of the supersonic airflow and solid surface of the ramjet inlet. Farther downstream, the airflow is further slowed down by the presence of the flame holders, as shown in the schematic in Figure 1.19. Downstream the ramjet inlet, the series of the oblique shock become normal shocks. As the airflow passes the flame holders, it enters the combustor where the combustion occurs. It is worth to mention here that the combustion products, in the form of hot gaseous flow, can reach high temperatures in the order of 2,400K. As the hot gases exit the combustor, the high temperature gas flow passes through the converging-diverging nozzle, as schematically shown in Figure 1.19. The sonic flow condition is achieved at the ramjet nozzle as shown in Figure 1.19. Farther downstream the nozzle, the flow accelerates due to the converging-diverging nozzle and thus, the airflow becomes supersonic as the flow passes the ramjet nozzle. Usually, the supersonic ramjets operate at high Mach numbers, reaching a maximum efficiency for Mach number M>3.

Chapter 2 Computational modeling of high-speed turbulent flows

2.1 Introduction to turbulence

2.2 Numerical methods

2.2.1 Direct numerical simulations (DNS)

$$\frac{\partial u_i}{\partial x_i} = 0 \tag{1}$$

$$\frac{\partial u_i}{\partial t} + \frac{\partial}{\partial x_j}(u_i u_j) = -\frac{\partial P}{\partial x_i} + \frac{1}{R_e}\frac{\partial^2}{\partial x_j^2} u_i \tag{2}$$

2.2.2 Large-eddy simulation (LES)

2.2.2.1 Governing equations

$$\frac{\partial \overline{u_i}}{\partial x_i} = 0 \tag{3}$$

$$\frac{\partial \overline{u_i}}{\partial t} + \frac{\partial}{\partial x_j}(\overline{u_i u_j}) = -\frac{\partial \overline{P}}{\partial x_i} + \frac{1}{R_e}\frac{\partial^2}{\partial x_j^2}\overline{u_i} \tag{4}$$

2.2.2.2 Smagorinsky model

$$\tau_{ij} - \frac{1}{3}\tau_{kk}\delta_{ij} = -\nu_T\left(\frac{\partial \overline{u_i}}{\partial x_j} + \frac{\partial \overline{u_j}}{\partial x_i}\right) = -2\nu_T\,\overline{S_{ij}} \tag{5}$$

where ν_T is called eddy viscosity and :

$$\overline{S_{ij}} = \frac{1}{2}\left(\frac{\partial \overline{u_i}}{\partial x_j} + \frac{\partial \overline{u_j}}{\partial x_i}\right). \tag{6}$$

2.2.2.3 Dynamic Smagorinsky model

$$\frac{\partial \tilde{\overline{u}}_i}{\partial t} + \frac{\partial}{\partial x_j}\left(\tilde{\overline{u}}_i\,\tilde{\overline{u}}_j\right) = -\frac{\partial \tilde{\overline{P}}}{\partial x_i} - \frac{\partial T_{ij}}{\partial x_j} + \frac{1}{R_e}\frac{\partial^2}{\partial x_j^2}\tilde{\overline{u}}_i \tag{7}$$

where $T_{ij} = \widetilde{\overline{u_i u_j}} - \tilde{\overline{u}}_i\,\tilde{\overline{u}}_j$.

$$\tau_{ij} - \frac{1}{3}\tau_{kk}\delta_{ij} \approx -2C_s\Delta^2\left|\overline{S}\right|\overline{S}_{ij} = -2C_s B_{ij} \tag{8}$$

$$T_{ij} - \frac{1}{3}T_{kk}\delta_{ij} \approx -2C_s\,\tilde{\Delta}^2\left|\tilde{\overline{S}}\right|\tilde{\overline{S}}_{ij} = -2C_s A_{ij} \tag{9}$$

$$L_{ij} = T_{ij} - \tilde{\tau}_{ij}\,. \tag{10}$$

$$E_{ij} = L_{ij} + 2C_s A_{ij} - 2C_s\,\tilde{B}_{ij} \tag{11}$$

$$E_{ij} = L_{ij} + 2C_s A_{ij} - 2C_s^* \tilde{B}_{ij} \,. \tag{12}$$

2.2.3 Improved delayed detached-eddy simulation (IDDES)

$$\frac{\partial(\rho k)}{\partial t} + \frac{\partial(\rho \mu_j k)}{\partial x_j} = \frac{\partial}{\partial x_j}\left[\left(\mu + \frac{\mu_t}{\partial_k}\right)\frac{\partial k}{\partial x_j}\right] + \tau_{ij} S_{ij} - \frac{\rho k^{1.5}}{L_{RANS}} \tag{13}$$

$$L_{IDDES} = \tilde{f}_d(1+f_e)L_{RANS} + (1-\tilde{f}_d)L_{LES} \tag{14}$$

where

$$L_{RANS} = \sqrt{k}/(\beta^* \omega) \tag{15}$$

$$L_{LES} = C_{DES} \times \Delta \tag{16}$$

$$\Delta = \min[\max(C_w \Delta_{\max}, C_w d, \Delta_{\min})\Delta_{\max}] \tag{17}$$

$$\Delta_{\min} = \min(\Delta x, \Delta y, \Delta z) \tag{18}$$

$$\Delta_{\max} = \max(\Delta x, \Delta y, \Delta z) \tag{19}$$

$$\tilde{f}_d = \max[(1-f_{dt}), f_B] \tag{20}$$

$$L_{IDDES} = \tilde{f}_d L_{RANS} + (1-\tilde{f}_d)L_{LES} \tag{21}$$

$$L_{IDDES} = f_B(1+f_e)L_{RANS} + (1-f_B)L_{LES} \tag{22}$$

2.3 Conclusions

The aerodynamics and thermodynamics of supersonic and hypersonic propulsion systems is associated with turbulent flows. Mathematical modeling of turbulence is still a challenging task and thus, accurate and computationally efficient mathematical models are needed. Therefore, the large-eddy simulation (LES) might be a promising approach for the numerical simulation of these kind of turbulent flows.

Chapter 3 Mach number effect on the aero-thermodynamics of subsonic, transonic and supersonic flights

3.1 Introduction

Supersonic cavity flows exhibit complex fluid dynamics such as, oscillating shear-layers, shock-shock and shock-boundary layer interactions [5-9]. In high-speed air-breathing propulsion, the supersonic mixing between fuel and air is of critical importance. The shock-boundary layer interactions may cause extinction of the flame, subsequently leading to catastrophic failure [5-9]. On the other hand, the flow features, of the free-stream velocity, play a key role in the efficient fuel-oxidizer mixing.

3.2 Computational method and models

3.2.1 Computational method

3.2.1.1 Large-eddy simulation (LES)

$$\frac{\partial \overline{u_i}}{\partial x_i} = 0 \tag{23}$$

$$\frac{\partial \overline{u_i}}{\partial t} + \frac{\partial}{\partial x_j}(\overline{u_i}\,\overline{u_j}) = -\frac{\partial \overline{P}}{\partial x_i} - \frac{\partial}{\partial x_j}\tau_{ij} + \frac{1}{R_e}\frac{\partial^2}{\partial x_j^2}\overline{u_i} \tag{24}$$

where $\tau_{ij} = \overline{u_i u_j} - \overline{u_i}\,\overline{u_j}$.[10-12]

$$L_{ij} = \overline{\tilde{u}_i \tilde{u}_j} - \overline{\tilde{u}_i}\,\overline{\tilde{u}_j} = T_{ij} - \bar{\tau}_{ij} \tag{25}$$

3.2.2 Computational model

Supersonic flow over a cavity of *L/D*=2, *W/D*=1 is numerically studied, where *L* is the streamwise length of cavity, *W* is spanwise length of cavity and *D* is the depth of cavity, as schematically shown in Figure 3.1.

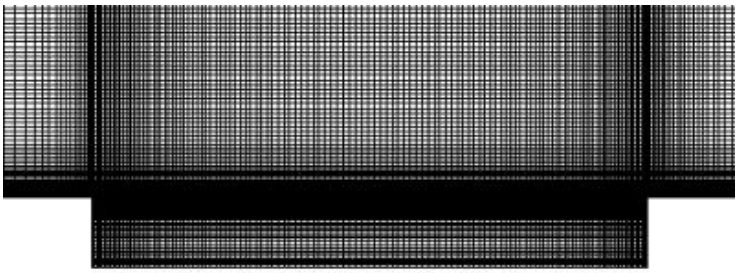

Figure 3.1 Computational domain

3.3 Results and discussion

Figure 3.13 presents the comparison of Mach number fields for supersonic (M=1.2) and transonic (M=0.9) cavity flows. Figure 3.13a presents the time-varying Mach number field, for supersonic flow, and the results reveal the presence of a large front of high-speed flow, as the supersonic flow enters the cavity. At the same time, two stagnation regions are identified at the bottom corners of the cavity, as shown in Figure 3.13a, at instant t=0.0006s.

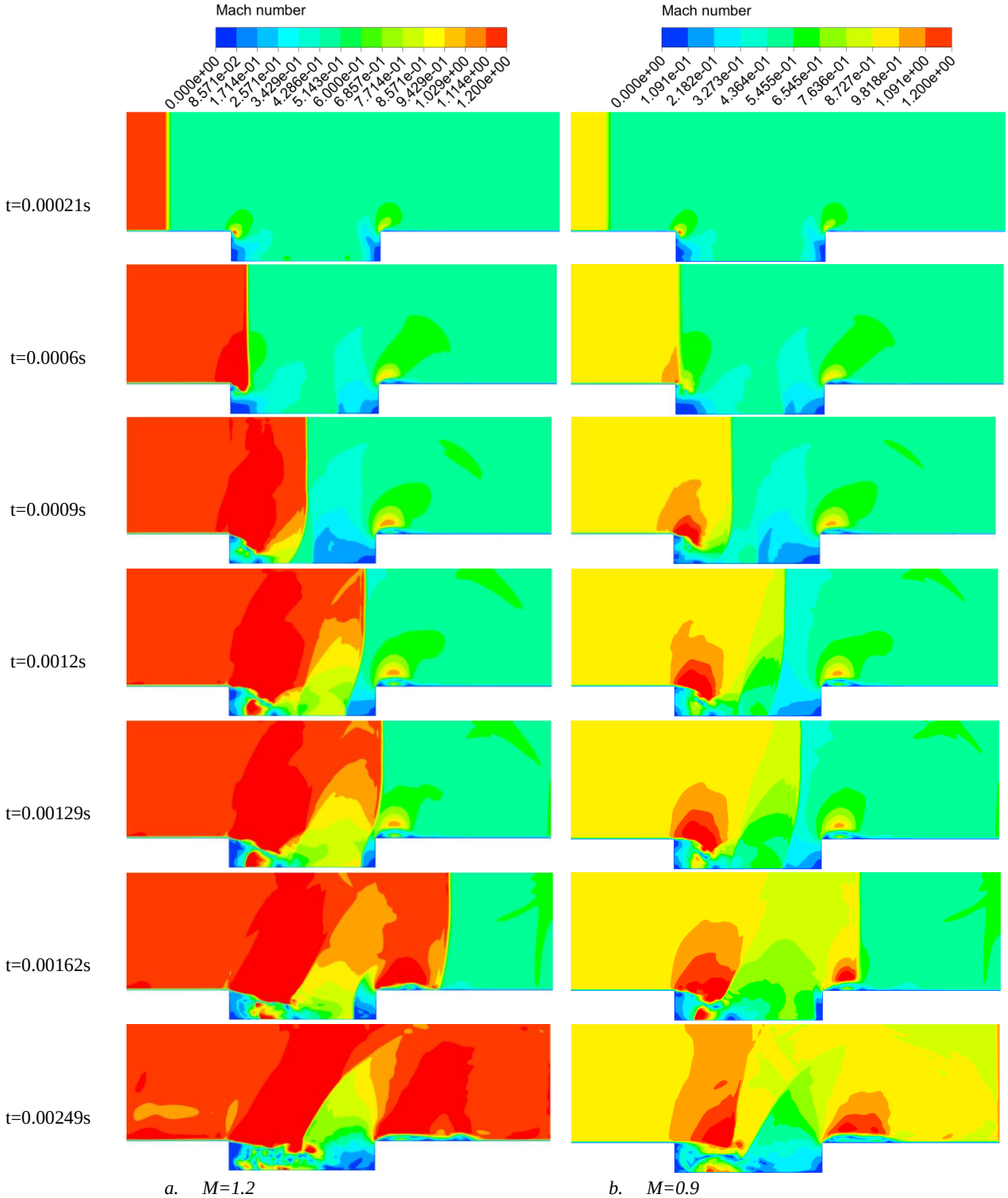

a. *M=1.2* *b.* *M=0.9*

Figure 3.2 Time-varying Mach number

As the supersonic flow advances farther, the stagnation flow regions grow in size, as shown in Figure 3.13, at instant t=0.0009s. As the supersonic flow enters the cavity region, there is a decrease in the flow-speed and implicitly in the Mach number, and this is well-illustrated in Figure 3.13a, at instant t=0.0012s.

The time-variation of the Mach number field, Figure 3.13, also shows that the initially supersonic flow becomes subsonic, as it enters the cavity and this is a desired flow condition for the combustion process (i.e. fuel residence-time and flame stabilization). The analysis reveals that as the front of the supersonic flow travels farther downstream, a relatively large flow recirculation region is formed near the rear-wall of the cavity, while smaller-size flow separation and recirculation zones are observed right after the fore-wall of the cavity. This is well-illustrated in Figure 3.13a, at instant t=0.0009s. As the front of the supersonic flow reaches the rear-wall of the cavity, the entire cavity is dominated by turbulent-mixing, while the stagnation regions, at the bottom corners, are still present as shown in Figure 3.13a, at instant t=0.00129s.

In the following, a more quantitative analysis of the supersonic, transonic and subsonic flow regimes will be presented. Thus, the Mach number effect on the flow variables is investigated at eight different locations inside the cavity, as shown in Figure 3.28.

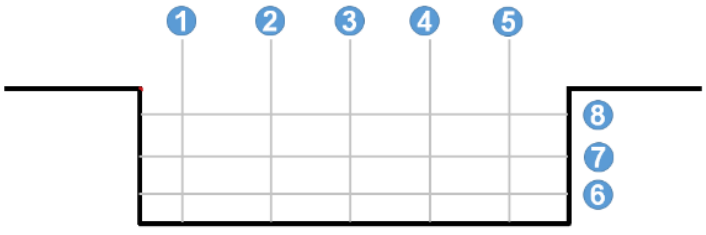

Figure 3.3 Interrogation locations of flow variables

Figure 3.29 presents the velocity field, for supersonic flow M=1.2, at five different locations inside the cavity, as schematically shown in Figure 3.28. The analysis reveals that there is an inversion

in the velocity magnitude and thus, the initially supersonic flow becomes subsonic inside the cavity. It is important to mention here that this is a desired flow regime for the combustion efficiency and stabilities. It is also important to mention here that the subsonic flow regime ensures the viability and stability of the flame. Also, the change in the flow regime from supersonic to subsonic ensures the turbulent-mixing inside the cavity, which plays a key role in the combustion process.

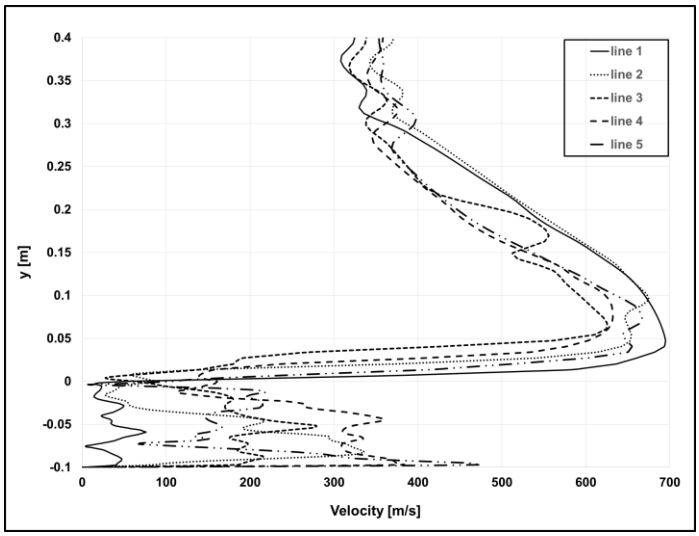

Figure 3.4 Velocity distribution inside the cavity; M=1.2

The analysis reveals that inside the cavity, the velocity reaches the lowest values in the regions of the fore and rear-walls of the cavity, while the largest values are attained in the middle of the cavity. The low velocity values, at these walls, are due to the stagnation condition of the impinging flow.

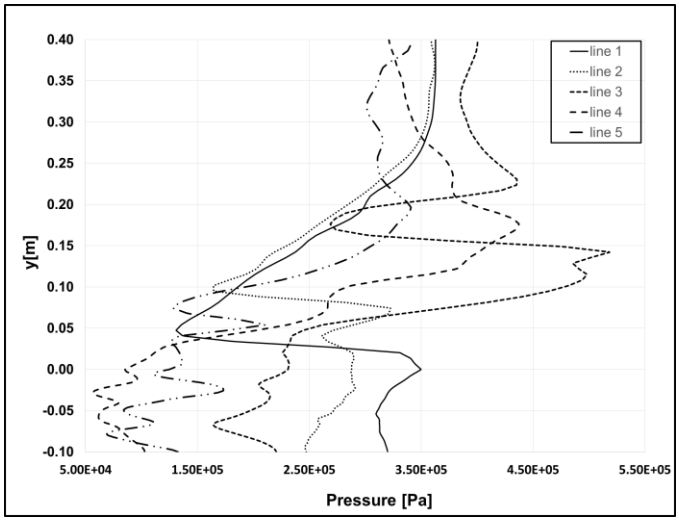

Figure 3.5 Pressure distribution inside the cavity; M=1.2

It is worth mentioning here that due to the flow recirculation inside the cavity, there is a continuous impingement of the flow on the fore and rear-walls of the cavity and thus, the velocity exhibits the lowest values at these locations. Moreover, the complex distribution of the velocity field, inside the cavity, is due to the high turbulent-mixing occurring inside the cavity. However, in the freestream region, the velocity decreases in the direction of the moving flow. Figure 3.30 presents the pressure field distribution inside the cavity, for supersonic flow M=1.2, at five different locations, as schematically shown in Figure 3.28. The analysis shows that, inside the cavity, the pressure reaches the highest values close to the fore and rear-walls of the cavity and this is also due to the flow impingement on these walls of the cavity. The pressure exhibits lower values farther upstream close to the fore-wall of the cavity. The analysis also shows that above the cavity there is an inversion in the pressure distribution due to the acoustics waves developed as a result of the interaction between the supersonic flow and cavity's rear-wall.

3.4 Conclusions

The analysis of the flow physics reveals the presence of a recirculation region, inside the cavity, and boundary layer detachment downstream the cavity. Due to the pressure unbalance within the

cavity an oscillating shear-layer is observed as well. The oscillating shear-layer spans the length of the open cavity and impinges on the aft wall. Shock-shock and shock boundary layer interactions are observed downstream the cavity. As a result of the shock-shock interaction, a lambda shock is observed as well.

Chapter 4 Performance enhancement of multi-disciplinary R&D teams through project management

4.1 Introduction

The past two decades have been characterized by profound changes and reallocations of human and material resources, worldwide, with implications in the dynamics of the companies and research institutions [1-11]. Therefore, nowadays, R&D may involve personnel located at various geophysical locations. In spite of their benefits, these changes raised significant challenges, particularly in terms of integrations, coordination and management of human resources, particularly for R&D teams [2, 4-7].

4.2 Analysis and discussion

The team performance is defined by three main elements, namely skills, commitment and accountability as shown in Figure 4.1. The individual's skills present different forms such as problem solving skills, technical and functional skills and interpersonal skills. The problem solving skills are key asset of any individual without which one cannot function and perform in a team.

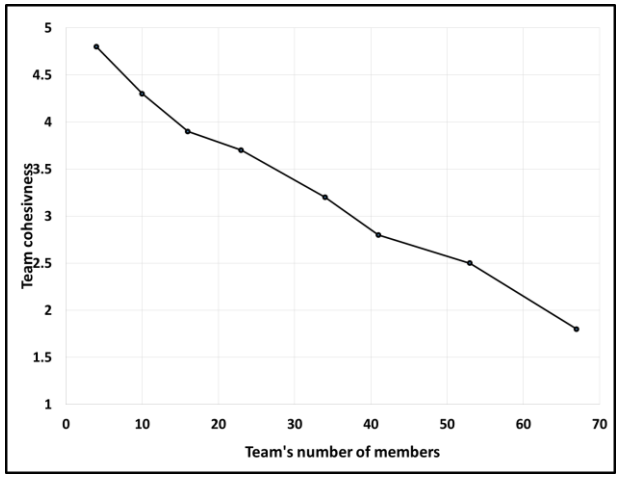

Figure 4.1 Cohesiveness of team function of team's members

4.3 Conclusions

In the present study, the factors affecting the performance of R&D teams are identified. Our study identified five different factors affecting the team performance, namely attendance, helpfulness, efficiency, initiative and quality.

Chapter 5 Computational modeling of human resources

5.1 Introduction

The group and team interactions have been of interest for many decades [1-3, 5-16]. Cultural difference may be the cause of unsuccessful completion of a goal or project [10, 12, and 16]. Personnel of different cultural backgrounds may or may not enhance the productivity of the team. Another important factor in the development and completion of research projects is the structure of the organization [7]. Thus, there are significant difference between the research performed in the corporate and academic environments. In corporations, the research is always aligned with the end product. Therefore, the deadlines for research completion are much stricter than in the

academic research setup. For the corporate research there is always a customer and a market that waits for the end product and thus, the research deadlines are more rigid. In the academic research there may or not be an end customer, depending on the type of research, fundamental or applied research. Therefore, the deadlines are somehow more relaxed and thus, less prone to conflicts associated with time contains. It is widely recognized that the communication is a major issue in any collaborative work and a major source of conflict generation. This could be encountered in the same team, organization or country.

5.2 Algorithms and mathematical modeling

In this research we focus on the modeling of teams as attractors and fractals. The Metropolis–Hastings algorithm generates a collection of states according to a desired distribution $P(x)$. This is accomplished when the Markov process convergences asymptotically to a stationary distribution of $\pi(x)$ such that $\pi(x) = P(x)$. Thus,

$$P(x^{'}|x)P(x) = P(x|x^{'})P(x^{'}) \tag{1}$$

which can be rewritten in the form

$$\frac{P(x^{'}|x)}{P(x|x^{'})} = \frac{P(x^{'})}{P(x)} \tag{2}$$

Based on the Metropolis acceptante ratio

$$A(x^{'}, x) = \min\{1, \frac{P(x^{'})}{P(x)} \frac{g(x|x^{'})}{g(x^{'}|x)}\} \tag{5}$$

A second approach employed in the current research is the Henon attractor/map which is a discrete-time dynamical system. The motivation for this model stems from the fact that it may predict the

chaotic behavior of the individual which may occur due to external perturbations. The Henon system of equation is defined as

$$\begin{cases} x_{n+1} = 1 - ax_n^2 + y_n \\ y_{n+1} = bx_n \end{cases} \quad (6)$$

The Henon map depends on two parameters a and b which for a chaotic map have the values $a = 1.4$ and $b = 0.3$.

5.3 Results and discussion

Figure 5.1 presents the correlation between the human factor and job availability. Thus, the red color data represents the response of human factor to the job availability, while the blue color graph represents the job availability. The model assumes that both the job availability and individual's attraction to the job availability varies in time. The delay between the individual' response and job availability is associated with the individual decision's uncertainty. It is common that human individual exhibit long term memory behavior, and thus, showing similar behaviors in time [5]. This is defined by the psychology of the individual and personality formation. Previous studies pointed out that this kind of behavior can be modeled as fractals. Thus, Figure 5.1b shows the fractal behavior of an individual. The fractal model is based on the Mandelbrot equations.

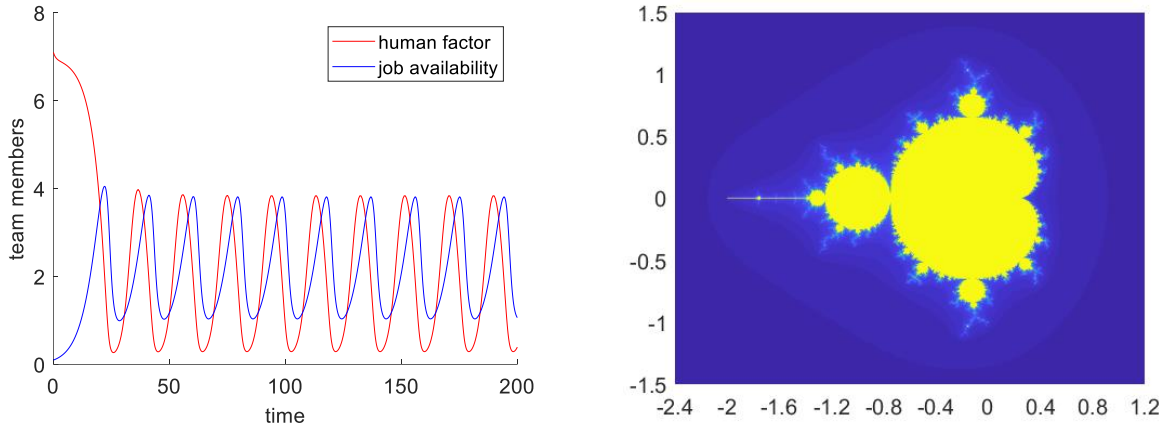

a. Attractor model

b. Fractal model

Figure 5.1 Attractor and fractal models

5.4 Conclusions

A computational model using the Metropolis–Hastings algorithm is developed for the modeling of dynamical systems. The present studies shows that the model provides accurate prediction of the system dynamics. The Henon attractor model is a promising approach for the numerical modeling of human resources as dynamical systems. The model offer the advantage of modeling highly chaotic systems and this occurs for values of $a = 1.4$ and $b = 0.3$. The Henon model shows that for small values of a and b variables, the system behaves chaotically.[122]

Chapter 6 Computational methods for the reduction and management of Big data in scientific computing

6.1 Introduction

The rapid progress in the developments of computing technologies and software such as high-performance computing (HPC) have generated large amounts of data that require further post-processing, interpretation and dissemination [1-5]. Post-processing and visualization of this large amount of data pose significant challenges, particularly when the data needs to be assembled/coupled form various instantaneous time frames [5, 6].

6.2 Computational modeling

The vorticity field is given by the determinant of the matrix given by equation 1:

$$\omega = \begin{bmatrix} \vec{i} & \vec{j} & \vec{k} \\ \frac{\partial}{\partial x} & \frac{\partial}{\partial y} & \frac{\partial}{\partial z} \\ u & v & w \end{bmatrix} \tag{1}$$

where u, v and w are the velocity components, corresponding to the vectors $\vec{i}$, $\vec{j}$, $\vec{k}$.

It is important to mention here that the mesh refinement is performed in the computing stage. The novelty of our approach comes from the fact that we perform the data filtering at the post-processing stage as well. This way we ensure the accuracy of the generated data as well facilitate the data management.

6.3 Results and discussion

A set of experimental data (pressure data) is presented in Figure 6.8a. As it can be seen from Figure 6.8b, the data contain some noise and we want to separate the good data from the noise data.

Performing an initial data filtering, we are able to separate the data based on the pressure values, Figure 6.8b. Further post-processing of data reduces even further the variance of the data, Figure 6.8c. The comparison between the experimental and computational data shows a very good agreement with the percentage error $\varepsilon \approx 5\%$. It is important to mention here that the AMR algorithm reduces the computational time by 72%.

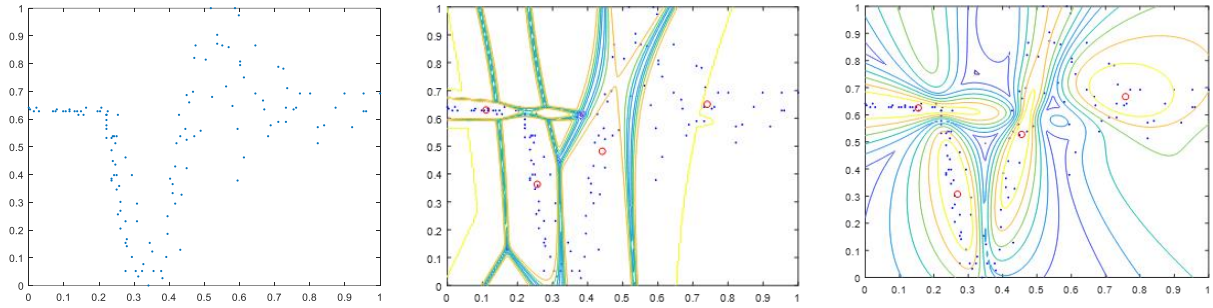

a. Data set *b. Data filtering* *c. Refinement of data*

Figure 6.1 Reduction of big data

6.4 Conclusions

An efficient computational approach for data management is developed to facilitate the post-processing of large-set of data. The data management approach comprises two different algorithms, namely the adaptive-mesh refinement and data filtering. The first algorithm reduces the number of the number of grid points of the computational domain, while the second algorithm filters the useful data. The comparison between the experimental and computational data shows very good agreement with a percentage error $\varepsilon \approx 5\%$.

Chapter 7 Conclusions, contributions and future research prospective

7.1 Conclusions

The present research focuses on the developments of aerospace engineering industry, specifically on the new developments of aircraft propulsion. The majority of the research in the aerospace industry, over the past decades, has focused on the developments of high-speed aircrafts, fuel efficiency and noise reduction. One of the main goals of aerospace industry has been the development of Scramjet aircrafts that would ensure high aerodynamic performance and stability, and fuel efficiency. Therefore, the main objective of this research is to address critical issues and further understanding of the aero-thermodynamics and aeroacoustics phenomena encountered in Scramjet propulsion. A second objective of the research concerns the development of mathematical algorithms for the computational modeling of the dynamics of human resources involved in multi-disciplinary research teams.

7.1.1 Chapter 1

- The literature review shows that there is a urgent need for the development of faster and aerodynamically performant aircrafts
- Over the past decades there have been significant efforts focused on the understanding of the supersonic combustion and high-speed air-breathing propulsion systems
- The literature review reveals the needs in the aerospace industry and research community for the development of high-fidelity computational approaches for the characterization of the aero-thermodynamics of supersonic flights and supersonic combustion
- One of the main computational challenges and needs concern the development of high-fidelity subgird-scale turbulence model for accurate characterization of complex turbulent flows
- From the flow physics perspective, the effect of the shocks, developed inside the cavity, on the flame stabilization and turbulent mixing are of high interest to the aerospace industry

7.1.2 Chapter 2

- Large-eddy simulation (LES) approach is a promising computational approach for the numerical prediction of highly turbulent flows
- The LES approach is suitable for the numerical computations of high-Reynolds number turbulent flows
- The LES offers the advantage of lower computational cost compared with the DNS and proving higher fidelity and time-dependent solution compared with the RANS approach

7.1.3 Chapter 3

- an improved delayed detached eddy simulation computational approach has been developed and employed in the numerical computations of highly turbulent flows
- the impact of flow Mach number on the aero-thermodynamics of cavity flow has been investigated for subsonic, transonic and supersonic flight conditions
- for all flight regimes, oblique shocks were observed that the front and rear upper corners of the cavity
- the intensity of these oblique shocks increase with the increase of the Mach number
- the temperature inside the cavity also increases with the increase of Mach number
- the open cavity contributes to the speed reduction of the supersonic flow and thus, it brings the supersonic flow at the subsonic flow regime which is need for the combustion stability

7.1.4 Chapter 4

- Chapter 4 concerns three different aspects of management namely (i) performance enhancement of multi-disciplinary R&D teams through project management, (ii) management of big data and (iii) computational modeling of human resources as dynamical systems
- One of the main objectives of this research is the performance enhancement of the multi-disciplinary research team.

- This research identified several factors that would affect the performance of the research team such as geographical location of the team members, cultural and societal, etc. another important factor that can impact the team performance and dynamics is the communication among the members of the team.

7.1.5 Chapter 5

- In this research probabilistic mathematical models were developed and implemented in the study of the human resources as dynamical systems.
- The Metropolis-Hasting algorithm along with Markov chain processes were employed in the analysis of the dynamics of human resources. A fractal model based on the Mandelbrot equations was also implemented and used in the study of the human resources dynamics.
- the research showed that the Metropolis-Hasting algorithm along with Markov chain can predict the dynamics of the human resources and thus, it helps in the project planning and being track with the milestone deadlines

7.1.6 Chapter 6

- an efficient algorithm was developed for the management of big data with particular application to the field of computational fluid dynamics
- the algorithm not only reduces the computational time but also facilitates the data post-processing
- the adaptive mesh refinement algorithm reduces the required grid points by the computational fluid dynamics solver and thus, a 70% computational time reduction is achieved
- a second algorithm is developed and used for the data post-processing. The algorithm is using a data filtering approach which enables faster post-processing of big data

7.2 Contributions

In spite of its known challenges, this research topics have given me the opportunity to bring my own contribution in the field of mathematical modeling related to the aerospace engineering and engineering management.

Therefore, my main contributions to the research community are listed below as follows:

- I developed a data filtering algorithm for the simplification of the data post-processing
- I developed a mathematical algorithm, based on the Metropolis-Hasting theory, for the modeling of human resources as dynamical systems
- I developed a Markov chain Monte Carlo (MCMC) algorithm for the mathematical modeling of dynamical systems

7.3 Future research prospective

As already mentioned, the focus of aerospace engineering research is on the development of high-speed aircraft carriers capable of providing aerodynamic stability, fuel efficiency and low noise and combustion emissions. The accomplishment of these objectives requires and opens new research opportunities that would enable a new era in the aerospace engineering.

One of the main research opportunity related to the high-speed air-breathing propulsion and in particular to Scramjet propulsion is the supersonic combustion. In spite of the extensive research, the supersonic combustion pose significant experimental and computational challenges. The experimental challenges stem from the fact that the equipment required by the experimental supersonic combustion are costly. On the other hand the computational challenges stem from the challenges posed by the numerical modeling of such complex turbulent flows characterized by a wide range of length and time scales.

Another research opportunity associated with the high-speed air-breathing propulsion is the aeroacoustics. The worldwide noise regulations requires extensive research to minimize the noise levels associated with the high-speed air-breathing propulsion.

Computational studies of the aero-thermodynamics of supersonic propulsion systems

A third research opportunity is related to the aero-elasticity phenomenon encountered in the high-speed flights. The aeroelasticity plays a critical role in the aerodynamic performance, structural integrity and aircraft stability. Therefore, the combustion, aeroacoustics and aeroelasticity associated with the high-speed air-breathing propulsion are the three main components that would requires extensive research in order to create a reliable and efficient high-speed aircraft.

Selected references

1. A.F. El-Sayed, Fundamentals of aircraft and rocket propulsion, Springer, 2016
2. M. Ihme, Combustion and Engine-Core Noise, Annu. Rev. Fluid Mech. 2017. 49:277–310
3. C. Soares, Gas Turbines (Second Edition), Pages 173-254, 2015
4. R. Paoli and K. Shariff, Contrail Modeling and Simulation, Annu. Rev. Fluid Mech., 48:393–427, 2016
5. J. Urzay, Supersonic Combustion in Air-Breathing Propulsion Systems for Hypersonic Flight, Annu. Rev. Fluid Mech., 50:593–627, 2018
6. Q. Liu, D. Baccarella, T. Lee, Review of combustion stabilization for hypersonic air-breathing propulsion, Progress in Aerospace Sciences 119, 100636, 2020
7. W. Huang, Transverse jet in supersonic crossflows, Aerospace Science and Technology 50, 183–195, 2016
8. T. Roos, A. Pudsey, M. Bricalli, H. Ogawa, Cavity enhanced jet interactions in a scramjet combustor, Acta Astronautica157, 162–179, 2019
9. S.J. Lawson, G.N. Barakos, Review of numerical simulations for high-speed, turbulent cavity flows, Progress in Aerospace Sciences 47, 186–216, 2011
10. M. Ilie, A. Semenescu, and M. Chan, Computational studies of turbine-stage, with variable inlet temperature; comparison between LES and IDDES,AIAA-2021-2522, 2021 AIAA Aviation Forum Conference, (virtual), 2–6 August, 2021
11. M. Ilie, A. Semenescu, M. Chan. "The effect of impinging jets on the turbulent mixing of cavity flows; numerical studies using LES and IDDES", AIAA AVIATION 2021 FORUM, 2021
12. M. Ilie, A. Semenescu, M. Chan and J. Asiatico, Combustion instabilities of swirl combustor with and without center-body air injection; computational studies using LES and IDDES, AIAA-2021-3481, 2021 AIAA Aviation Forum Conference, (virtual), 2–6 August, 2021
13. M. Ilie, A. Semenescu, G. L. Stroe, S. Berbente, Numerical computations of cavity flows using the potential flow theory, Annals of the Academy of Romanian Scientists, Series on Engineering Sciences, ISSN 2066-8570, Vol. 13, Nr. 2, 2021
14. M. Ilie, A. Semenescu, G. L. Stroe, S. Berbente, Computational studies of turbulent cross-flow jet using LES, Annals of the Academy of Romanian Scientists, Series on Engineering Sciences, ISSN 2066-8570, Vol. 13, Nr. 2, 2021
15. M. Ilie, A. Semenescu, G. L. Stroe, S. Berbente, A computational combustion method for turbulent pulverized solid fuel using LES, Annals of the Academy of Romanian Scientists, Series on Engineering Sciences, ISSN 2066-8570, Vol. 13, Nr. 2, 2021
16. M. Ilie, A. Semenescu, Aerodynamic studies of aircraft engine turbine stage, Annals of the Academy of Romanian Scientists, Series on Engineering Sciences, ISSN 2066-8570, Vol. 14, Nr. 2, 2022

17. M. Ilie, A. Semenescu, Computational studies of aeroelasticity of aircraft engine turbine blade, Annals of the Academy of Romanian Scientists, Series on Engineering Sciences, ISSN 2066-8570, Vol. 14, Nr. 2, 2022
18. M. Ilie, A. Semenescu, Computational studies of helicopter aerodynamics, Annals of the Academy of Romanian Scientists, Series on Engineering Sciences, ISSN 2066-8570, Vol. 14, Nr. 2, 2022
19. M. Ilie, A. Semenescu, Winglet effect on the aerodynamics of aircraft wing; computational studies, Annals of the Academy of Romanian Scientists, Series on Engineering Sciences, ISSN 2066-8570, Vol. 14, Nr. 2, 2022
20. M. Ilie, M. Chan and J. Asiatico, Combustion instabilities in backward- step premixed reacting flows; computational studies using LES, AIAA- 2022-9438, 2022 AIAA SciTech Conference, San Diego, CA, 3–7 January, 2022
21. M. Ilie, M. Chan, J. Asiatico, Supersonic combustion of scramjet jet cavity with ramp; computational studies using LES, AIAA 2023-1648, 2023 AIAA SciTech Conference, National Harbor, MD, 23–27 January 2023
22. M. Ilie, M. Chan, J. Asiatico, Thermoacoustic instabilities of coaxial jet combustor; computational studies using LES, AIAA 2023-1063, 2023 AIAA SciTech Conference, National Harbor, MD, 23–27 January 2023
23. M. Ilie, M. Chan and J.Asiatico Numerical computations of turbulent swirling reacting flows using IDDES, AIAA-2022-4164, 2022 AIAA Aviation Forum Conference, Chicago, IL,27 June–1 July, 2022
24. M. Ilie, M. Chan and J.Asiatico, Computational studies of turbulent reacting flows in rear-wall expansion cavity using LES, AIAA-2022-4046, 2022 AIAA Aviation Forum Conference, Chicago, IL, 27 June–1 July, 2022
25. M. Ilie, M. Chan and J. Asiatico, Combustion instabilities in backward- step premixed reacting flows; computational studies using LES, AIAA- 2022-9438, 2022 AIAA SciTech Conference, San Diego, CA, 3–7 January, 2022
26. M. Ilie, J. Asiatico and M. Chan, Active flow control, for fixed wings, using synthetic jets, AIAA-2022-9369, 2022 AIAA SciTech Conference, San Diego, CA, 3–7 January, 2022
27. M. Ilie, J. Asiatico and M. Chan, Combustion instabilities of swirl combustors, with radial and axial air injection schemes; computational studies using LES and IDDES, AIAA-2021-3571, 2021 AIAA Aviation Forum Conference, (virtual), 2–6 August, 2021
28. M. Ilie, A. Semenescu, G. L. Stroe, S. Berbente, Numerical computations of cavity flows using the potential flow theory, Annals of the Academy of Romanian Scientists, Series on Engineering Sciences, ISSN 2066-8570, Vol. 13, Nr. 2, 2021
29. G. N. Barakos, S.J. Lawson, R. Steijl, P. Nayyar, Numerical simulations of high-speed turbulent cavity flows. Flow Turbul. Combust 83, 569–585, 2009
30. F. W. Barnes, C. Segal, Cavity-based flame holding for chemically-reacting supersonic flows, Progress in Aerospace Sciences, 76, 24–41, 2015
31. M. Germano, U. Piomelli, P. Moin, and W. H. Cabot, A dynamic subgrid-scale eddy viscosity model, Phys. Fluids A 3 (7), 760-1765, 1991
32. D.H. Kim, J.H. Choi, O.J. Kwon, Detached eddy simulation of weapons bay flows and store separation, Comput. Fluids 121, 1–10, 2015
33. L. Larchevêque, P. Sagaut, I. Mary, and O. Labbé, Large-eddy simulation of a compressible flow past a deep cavity. Physis of Fluids, 15(1), 2003
34. L. Larcheveque, P. Sagaut, T-H. Le, P. Comte, Large-eddy simulation of a compressible flow in a three-dimensional open cavity at high Reynolds number, J. Fluid Mech., 516, 265–301, 2004
35. S.J. Lawson, G.N. Barakos, Review of numerical simulations for high-speed, turbulent cavity flows, Prog. Aerosp. Sci., 47, 186–216, 2011
36. Chen, Y., Li, S.X., Group identity and social preferences. Am. Econ. Rev. 99 (1), 431–457, 2009

37. Eckel, C.C., Grossman, P.J., Managing diversity by creating team identity. J. Econ. Behav. Organiz. 58 (3), 371–392, 2005
38. Hamilton, B.H., Nickerson, J.A., Owan, H., Team incentives and worker heterogeneity: An empirical analysis of the impact of teams on productivity and participation. J. Polit. Econ. 111 (3), 465–497, 2003
39. Ichniowski, C., Shaw, K., The effects of human resource management systems on economic performance: An international comparison of US and Japanese plants. Manage. Sci. 45 (5), 704–721, 1999
40. DeChurch, L. A., and Mesmer-Magnus, J. R., The cognitive underpinnings of effective teamwork: a meta-analysis. J. Appl. Psychol. 95, 32–53, 2010
149. https://en.wikipedia.org/wiki/Glider_%28sailplane%29
150. https://commons.wikimedia.org/wiki/File:419th_Flight_Test_Squadron_-_B-2_Spirit.jpg
151. https://en.wikipedia.org/wiki/Boeing_X-48
155. https://themechanicalengineering.com/turbojet-engine/
157. https://en.wikipedia.org/wiki/Ramjet